

Observation of Nonzero θ_{13} at Reactor Antineutrino Experiments

H.R. Band ¹, on behalf of the Daya Bay Collaboration

University of Wisconsin

Madison, WI, USA

E-mail: hrb@slac.stanford.edu

The Daya Bay Reactor Neutrino Experiment was the first to observe a non-zero value for the neutrino mixing angle θ_{13} with a significance of 5.2 standard deviations this spring. The RENO experiment confirmed this observation one month later. Recently Daya Bay and Double Chooz have announced updated results. The status of these reactor antineutrino experiments is summarized.

*The XIth International Conference on Heavy Quarks and Leptons,
Prague, Czech Republic
June 11-15, 2012*

¹ Speaker

1. Introduction

The neutrino mixing angle θ_{13} , the last unmeasured angle in the neutrino mass matrix [1,2], was observed with $> 5.2\sigma$ significance by the Daya Bay Reactor Neutrino Experiment [3] in the spring of 2012. The RENO Experiment confirmed this result a month later [4]. These experiments followed the first indications of non-zero θ_{13} by both accelerator [5,6] and reactor [7] based experiments the previous winter. Recently Daya Bay [8] and Double Chooz [9] have reported improved measurements based on larger data sets. The status of these reactor antineutrino experiments is described.

Neutrino oscillations were well established in muon-type neutrinos by measurements from SuperK (atmospheric) [10] and K2K (accelerator) [11]. Oscillations in electron-type neutrinos explained the solar neutrino deficit, which was first observed by Davis [12] and was accurately measured by SNO [13], solar SK [14], and KamLand [15]. Our understanding of the observed mixing values is captured by the unitary 3 by 3 neutrino mass matrix (U_{MNSP}) [1,2] which relates the neutrino lepton flavor eigenstates to the mass eigenstates. Unlike the CKM matrix in the quark sector the MNSP matrix contains large off-diagonal terms. If neutrinos are Dirac particles, the matrix contains three mixing angles, two mass terms and a complex phase determining CP violation. Prior to this year only θ_{13} and the CP phase were unmeasured. Accurate knowledge of θ_{13} is needed to plan future experiments measuring the neutrino mass hierarchy or CP violation in the neutrino mass matrix.

The probability that an electron type antineutrino would be observed as an electron type antineutrino some distance away is given by:

$$P_{ee} \approx 1 - \sin^2 2\theta_{13} \sin^2 \left(\frac{\Delta m_{31}^2 L}{4E_\nu} \right) - \cos^4 \theta_{13} \sin^2 2\theta_{12} \sin^2 \left(\frac{\Delta m_{21}^2 L}{4E_\nu} \right)$$

L is the distance in kilometers of the measurement, E is the neutrino energy in MeV, θ_{12} and θ_{13} are the mixing angles, and Δm_{31}^2 and Δm_{21}^2 are the square of the mass differences between the neutrino mass states. Given the current measured mixing parameters (θ_{12} , Δm_{31}^2 , Δm_{21}^2) the survival probability is shown in Fig. 1a assuming that $\sin^2 2\theta_{13} = 0.10$.

Antineutrinos are detected via inverse beta-decay (IBD) reactions $\bar{\nu}_e + p \Rightarrow e^+ + n$ on the hydrogen rich liquid scintillator target. This reaction has a 1.8 MeV threshold on free protons. The observed energy spectrum, shown in Fig. 1b [16], has an average energy of 3.6 MeV. IBD

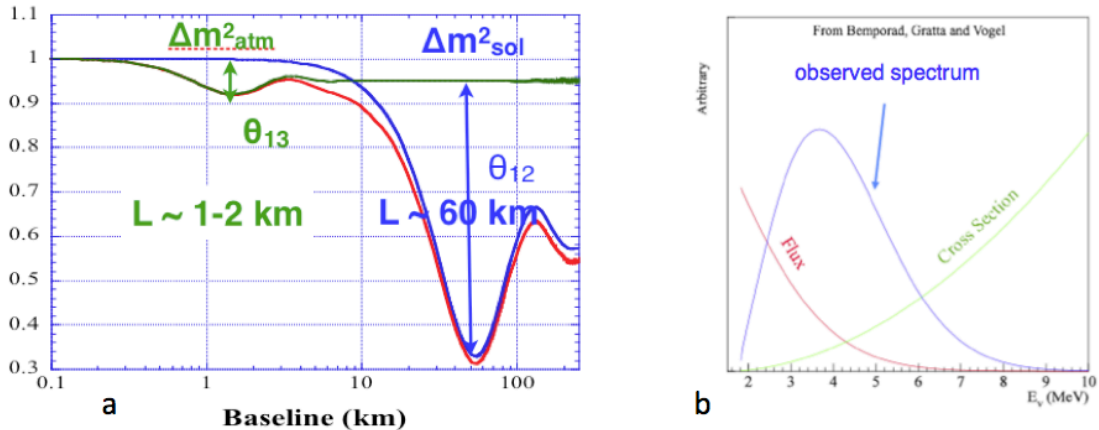


Figure 1. (a) The fraction of reactor antineutrinos detectable in inverse beta decay interactions (IBD) are shown as a function of baseline. (b) The observed energy spectrum of these antineutrinos is the convolution of the rapidly falling energy spectrum of reactor neutrinos with the rising IBD cross-section.

events are characterized by a prompt signal from the positron annihilation ($E > 1.02$ MeV) followed by a delayed signal from neutron capture on gadolinium (8.05 MeV). The antineutrino energy is determined from the positron energy.

This paper describes accurate measurements of θ_{13} using electron type anti-neutrinos from nuclear reactors. A non-zero θ_{13} causes a small deviation from the expected $1/r^2$ behavior in the number of antineutrino interactions observed as a function of distance from the reactor core. Measuring the antineutrino flux at two distances from the core as suggested by Mikaelyan and Sinev[17] eliminates many systematic errors which limited the precision of previous single detector measurements. The measured ratio between antineutrino rates at the near and far sites is insensitive to absolute reactor flux predictions and detector efficiencies. Only relative differences between the detector efficiencies are important. These differences are minimized by building nearly identical detectors at the near and far sites and by filling them with identical liquids.

The Daya Bay experiment measures the antineutrino flux from 6 high power (2.9 GW_{th}) commercial nuclear reactors at the Daya Bay Power Plant at varying distances from the reactor cores with six antineutrino detectors (AD) as shown in Fig. 2. Each of two near detector halls contains one or two ADs in a common water pool. The far experimental hall contains three ADs in a water pool. The average flux-weighted distance between the detectors and the pair of reactor cores is approximately 470 m for EH1, 576 m for EH2, and 1648 m for EH3. In late summer 2012, two more ADs will be installed.

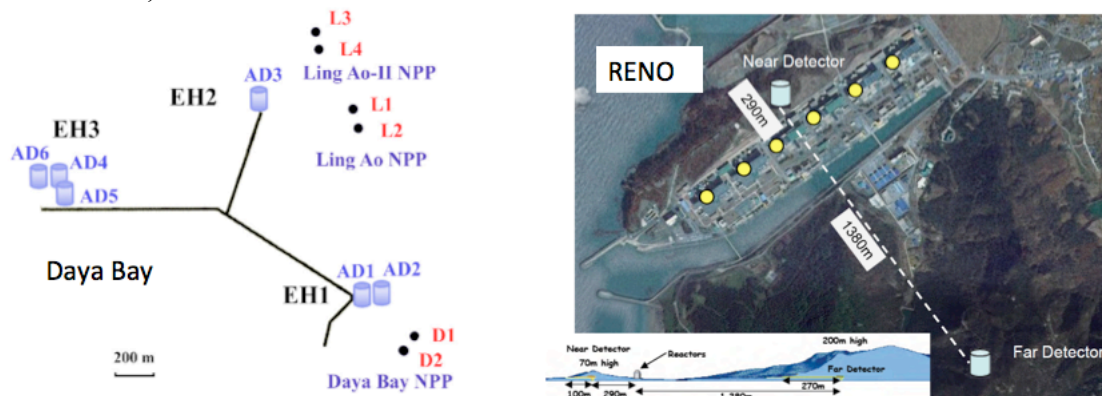


Figure 2. (left) Layout of the Daya Bay experiment. The dots represent reactors, labeled as D1, D2, L1, L2, L3 and L4. Six ADs, AD1-AD6, are installed in three EHs. (right) Layout of the RENO experiment. The six reactors (yellow dots) are aligned on a straight line. The near and far detectors are on opposite sides of the reactors

The RENO experiment has single far and near detectors monitoring six high power (2.7 GW_{th}) reactors as shown in Fig. 2. The near detector is 290 m from the straight line on which the reactor cores are aligned. The far detector is 1380 m from this line. Both the near and far detectors have a target mass of 16.5 tons. Although a near detector is planned for the Double Chooz experiment (not shown), results to date are based on a single detector of approximately 8 tons located 1050 m from two 4.7 GW_{th} reactor cores. The Daya Bay detectors and analysis are described next as representative of these reactor antineutrino experiments.

2. Daya Bay Detector

Each AD consists of a Stainless Steel Vessel (SSV) containing three detector zones filled with different liquids as shown in Fig. 3. Two nested acrylic cylinders separate the three zones. The innermost target zone containing 20 tons of gadolinium doped liquid scintillator (GdLS) inside an Inner Acrylic Vessel (IAV) is surrounded by 21 tons of liquid scintillator (LS)

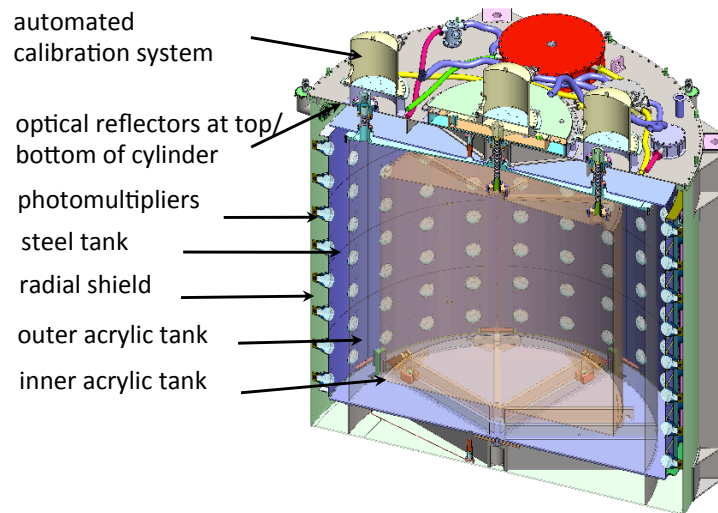


Figure 3. Daya Bay antineutrino detector.

gamma catcher contained by an Outer Acrylic Vessel (OAV). An outer zone containing 37 tons of mineral oil (MO) shields the inner zones from the radioactivity of the glass PMTs and other background sources. Energy from IBD interactions is observed by 192 PMTs (Hamamatsu R5912) arranged in a cylindrical shell. Reflectors above and below the LS volume improve the light detection efficiency.

Three automated calibration units (ACU) above the SSV lid allow remote deployment of radioactive sources or LED flashers into the GdLS or LS liquid volumes. Each ACU is equipped with an LED, a ^{68}Ge source, and a combined source of $^{241}\text{Am-C}$ and ^{60}Co . Weekly calibration data runs are interspersed with normal data to accurately measure and track the energy response of each AD.

The liquid scintillator is linear alkyl benzene with 3 g/L PPO and 15 mg/L bis-MSB fluorescing agents added. Gadolinium chloride reacts with 3,5,5-trimethylhexanoic acid (TMHA) to form a solid complex $\text{Gd}(\text{TMHA})_3$ that dissolves in LAB. The Gd-LS has 87.7% carbon content by weight, 12.1% hydrogen, and 0.103% Gd. The densities of the Gd-LS, LS, and mineral oil are 0.860, 0.859, and 0.851 g/ml, respectively.

ADs are assembled in pairs above ground in a large class-10,000 clean room before moving underground to be filled simultaneously with all three liquids. Liquid masses are measured with Coriolis flow meters. The Gd-LS is first pumped into a Teflon-lined tank instrumented with load cells. Comparing the load cell measurements before and after filling, determine the Gd-LS target mass to 0.02%. AD pairs are filled back to back to ensure that liquid properties are identical as possible.

The ADs sit in water pools which shield the detectors with > 2.5 m of water in all directions from ambient radioactivity as shown in Fig. 4. PMTs are arranged in optically separated inner (IWS) and outer water (OWS) pool zones to detect muons, which may introduce spallation neutrons or other cosmogenic backgrounds into the ADs. Four layers of Resistive Plate Chambers (RPCs) added redundant cosmic ray detection, but have not yet been used in reported analyses.

PMT signals from the ADs and water pool zones are routed separately out of the water to VME crates containing ADCs and TDCs. With PMT charge gains adjusted to $\approx 1 \cdot 10^7$, the average AD dark rate was 10 kHz per PMT. The AD trigger rates varied from 140-280 Hz. AD energy and multiplicity thresholds were measured to be ≈ 0.4 MeV and were fully efficient for positrons from IBD events (> 1.0 MeV). About 5% of AD triggers were caused by light emitted from some of the PMT bases (flashers). These events were easily identified by geometric and

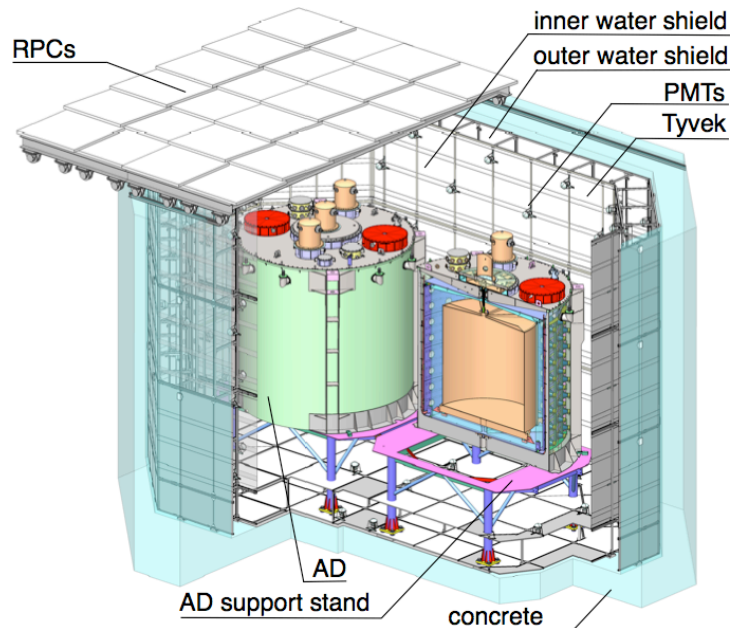


Figure 4. Schematic diagram of 2 Daya Bay ADs in one of the near experimental halls. The components of the dual water shield are indicated.

PMT deposition patterns and are eliminated from the analysis sample. The inner and outer water pool zones were triggered by a multiplicity trigger ($n_{hit} > 12$). Typical trigger rates for the IWS (OWS) were 125 (210) Hz in the near experimental halls and < 25 Hz in the far hall. Muon detection efficiency was 99.7% for the IWS and 97% for the OWS.

3. Daya Bay Analysis

Time correlated events are identified by requiring a prompt energy signal ($E_p > 0.7$ MeV) followed by a delayed energy signal ($E_d > 0.7$ MeV) 1-200 μ sec later. Events within one msec of a muon signal in the AD ($E > 20$ MeV) or within 1 second of a showering muon ($E > 2.5$ GeV) were discarded. A scatterplot of correlated events shown in Fig. 5 clearly show delayed neutron captures from IBD events on Gd (8.05 MeV) and hydrogen (2.2 MeV). Antineutrino candidates were required to have $0.7 < E_p < 12.0$ MeV and $6.0 < E_d < 12.0$ MeV as shown by the box in Fig. 5. Further cuts ensured that there was no activity within 200 μ sec in the surrounding water pool. A final cut ensured there was only one pair of energy depositions in the chosen time window.

The updated Daya Bay data set was taken from Dec. 24, 2011 to May 11, 2012. Only data with all three halls operational were included. The live time after the muon related analysis cuts was calculated by integrating the time between muon vetoes for each AD. Since the muon rate varied significantly between experimental halls, the efficiency (ϵ_μ) varied from 0.80 in EH1 to 0.90 in EH3. Table 1 shows the number of antineutrino candidates, backgrounds, and calculated rates for the updated Daya Bay data set.

The largest background in the antineutrino candidate sample is from the accidental coincidence of two uncorrelated single energy depositions from radioactive backgrounds. Since the singles spectrum falls sharply with energy most of these events have very low prompt energy. The rate of these events is very well modeled by studies of out of time random coincidences. True time-correlated backgrounds are much smaller and include fast neutrons and

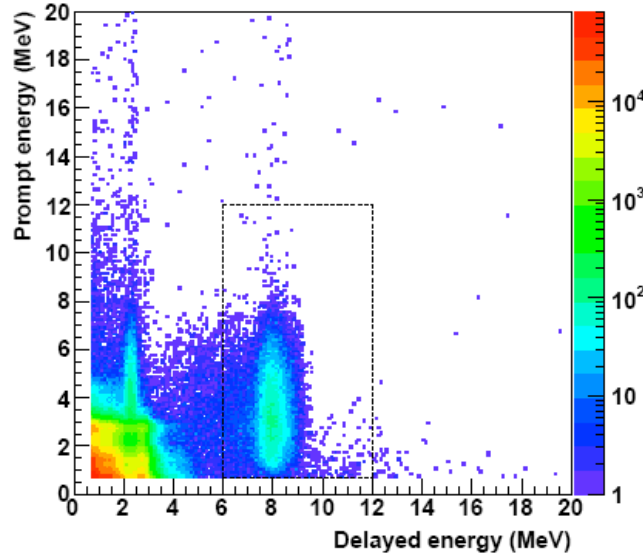


Figure 5. Scatter plot of the energy of prompt-delayed pairs. Events inside the dotted line box are taken as IBD candidates.

${}^8\text{He}/{}^9\text{Li}$ decays that are produced by cosmic ray muons.

Accurate knowledge of the relative detection efficiency of the near and far ADs is crucial for comparing the antineutrino fluxes at different baselines. Numerous crosschecks confirmed the near-identicalness of the ADs [18]. For example, the time between the prompt and delayed signals depends sensitively on the number Gd and hydrogen nuclei. Fits to the measured neutron capture time showed that all detectors have consistent IBD capture times limiting variations in the Gd concentration to $< 0.1\%$.

| | AD1 | AD2 | AD3 | AD4 | AD5 | AD6 |
|----------------------------------------------------|-------------------------------------|-------------------------------------|-------------------------------------|------------------------------------|------------------------------------|------------------------------------|
| Antineutrino candidates | 69121 | 69714 | 66473 | 9788 | 9669 | 9452 |
| DAQ live time (day) | 127.5470 | | 127.3763 | | 126.2646 | |
| Efficiency | 0.8015 | 0.7986 | 0.8364 | 0.9555 | 0.9552 | 0.9547 |
| Accidentals (/day) | 9.73 ± 0.10 | 9.61 ± 0.10 | 7.55 ± 0.08 | 3.05 ± 0.04 | 3.04 ± 0.04 | 2.93 ± 0.03 |
| Fast neutron (/day) | 0.77 ± 0.24 | 0.77 ± 0.24 | 0.58 ± 0.33 | 0.05 ± 0.02 | 0.05 ± 0.02 | 0.05 ± 0.02 |
| ${}^8\text{He}/{}^9\text{Li}$ (/day) | 2.9 ± 1.5 | | 2.0 ± 1.1 | | 0.22 ± 0.12 | |
| Am-C corr. (/day) | 0.2 ± 0.2 | | | | | |
| ${}^{13}\text{C}(\alpha, n){}^{16}\text{O}$ (/day) | 0.08 ± 0.04 | 0.07 ± 0.04 | 0.05 ± 0.03 | 0.04 ± 0.02 | 0.04 ± 0.02 | 0.04 ± 0.02 |
| Antineutrino rate (/day) | 662.47 ± 3.00 | 670.87 ± 3.01 | 613.53 ± 2.69 | 77.57 ± 0.85 | 76.62 ± 0.85 | 74.97 ± 0.84 |

Table 1. Breakdown of the number of candidate and background events measured during the updated Daya Bay data run from Dec. 24, 2011 to May 11, 2012.

Only relative systematic errors in the detection efficiency are important. Thus uncertainties in the fraction of antineutrino events originating outside of the GdLS volume (absolute uncertainty of 1.5%), the fraction of events that capture on gadolinium (abs. uncertainty of 0.8%), or in the number of target protons in the GdLS (abs. uncertainty of 0.5%) are nearly cancelled in the ratio of detector efficiencies ($< 0.03\%$). The overall AD detection efficiency is 78.8% and is known with a systematic error of 1.9%. Variations in the relative

detection efficiency are dominated by differences in the detector mass, 0.5%, but are known to 0.2%.

The expected antineutrino rate of each AD was predicted as a function of time using the flux from each reactor, the measured distances between reactors and detectors and a Monte Carlo simulation of the detector. The reactor flux predictions [3] utilized thermal power information and core composition fractions from the nuclear power plants and the antineutrino spectrum and energy released per fission. Most of the systematic uncertainties in the predicted flux were correlated between reactors (3%), while uncorrelated uncertainties that would contribute to a near/far measurement were much smaller (0.8%). Fig. 6 shows the average IBD rates from each EH as a function of time. The predicted IBD rates are shown for comparison assuming no neutrino oscillation (dashed line) or with the measured oscillation (black line). Both predictions allow the total reactor flux to float within the correlated error. Changes in the observed flux during reactor shutdowns for refuelling are clear. It is also evident that the no oscillation scenario over predicts the number of events at the far hall. The ratio of observed to expected events at the far hall (no oscillation) is $R = 0.944 \pm 0.007(\text{stat}) \pm 0.003(\text{syst})$.

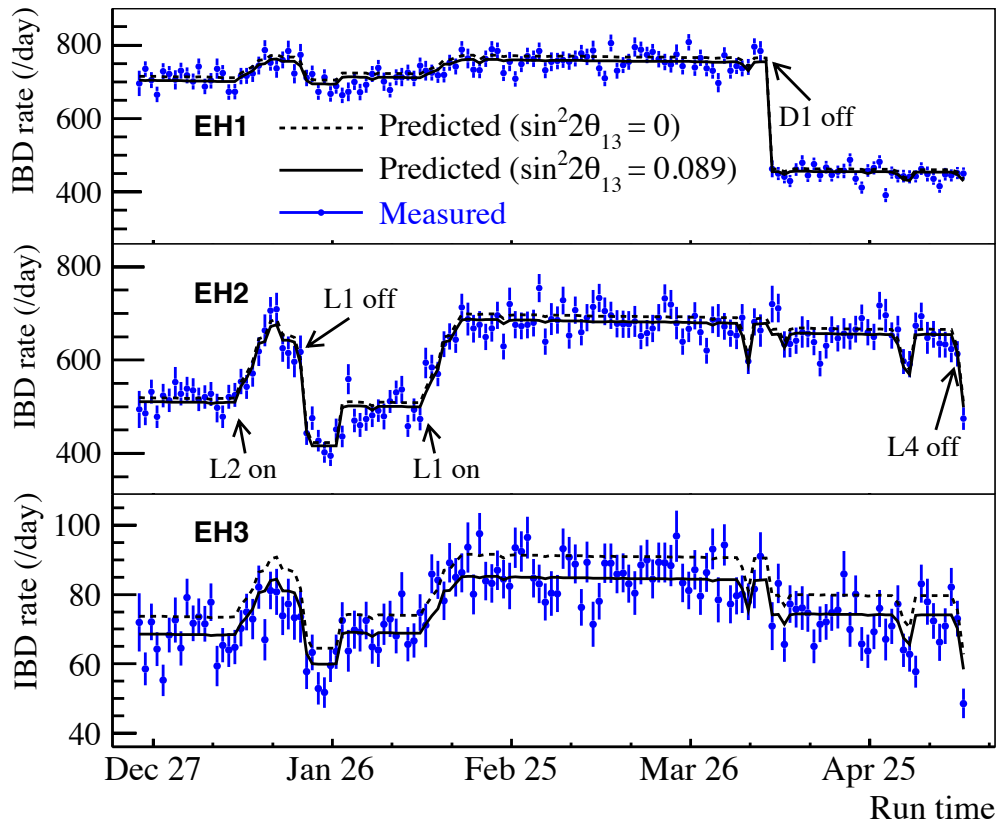


Figure 6. Daya Bay. Daily average measured IBD rates per AD in the three experimental halls as a function of time. The dashed curves are no-oscillation predictions based on reactor flux analyses and detector simulation. The solid black line curves are the predictions corrected by the best-fit $\sin^2 2\theta_{13}$.

The value of $\sin^2 2\theta_{13}$ was determined by minimizing a standard χ^2 function that included pull terms accounting for the correlation of the systematic errors. The best-fit value is $\sin^2 2\theta_{13} = 0.089 \pm 0.010(\text{stat}) \pm 0.005(\text{syst})$. The no oscillation hypothesis is excluded at 7.7 standard deviations. Fig. 7 shows the measured versus expected number of events for each AD as a function of the flux weighted average distance of each AD from the reactor cores. With no oscillation, a flat line at 1.0 is expected. The best-fit oscillation prediction is given by the smooth curve. The χ^2 value versus $\sin^2 2\theta_{13}$ is shown in the inset.

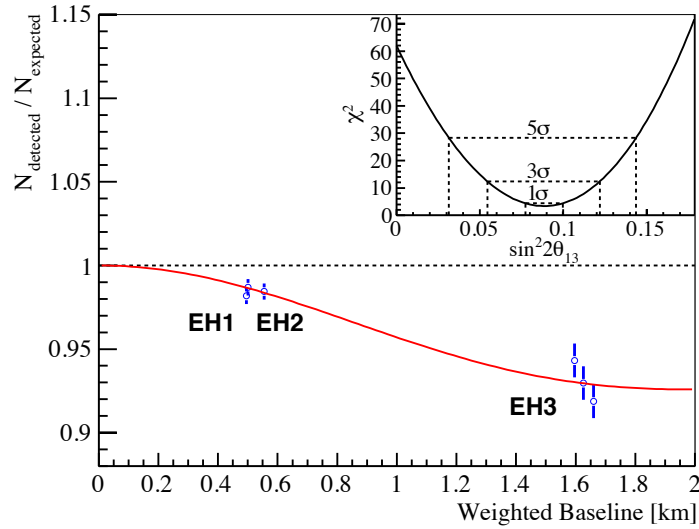


Figure 7. Measured versus expected signal ratios in each detector are shown, assuming no oscillation. Reactor and survey data are used to compute the flux-weighted average baselines. The oscillation survival probability at the best-fit value is given by the smooth curve, corrected with the best-fit normalization parameters. The AD4 and AD6 data points are displaced by -50 and +50 m for visual clarity. The χ^2 versus $\sin^2 2\theta_{13}$ is shown in the inset.

The average prompt energy spectrum observed by the three ADs in the far hall is shown in the upper half of Fig. 8. A predicted spectrum based on a weighted combination of near hall spectra is also shown. The ratio of the spectra are shown in the lower plot compared with the predicted ratio assuming no oscillation (dashed line) or the best-fit oscillation $\sin^2 2\theta_{13} = 0.089$ (red curve).

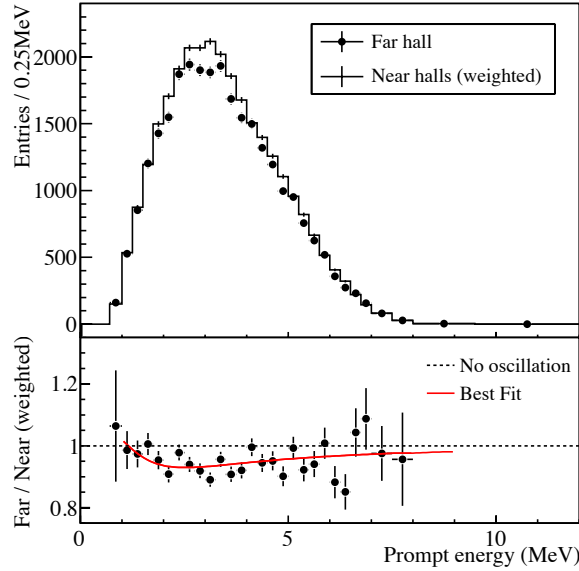


Figure 8. Top: Measured prompt energy spectrum of the far hall (sum of three ADs) comparing to the no-oscillation prediction from the measurements of the two near halls. Both are background subtracted. Uncertainties are statistical only. Bottom: The ratio of measured and predicted no-oscillation spectra. The red curve is the best-fit solution with $\sin^2 2\theta_{13} = 0.089$ obtained from the rate-only analysis. The dashed line is the no-oscillation prediction.

4. Double Chooz and Reno

Double Chooz updated their result at the Neutrino 2012 conference [9] with a rate plus shape analysis yielding $\sin^2 2\theta_{13} = 0.109 \pm 0.030(\text{stat}) \pm 0.025(\text{syst})$. The RENO result [4] from a rate only analysis remains $\sin^2 2\theta_{13} = 0.113 \pm 0.013(\text{stat}) \pm 0.019(\text{syst})$. The world measurements of $\sin^2 2\theta_{13}$ are shown in Fig. 9. [19]. The Daya Bay result, $\sin^2 2\theta_{13} = 0.089 \pm 0.010(\text{stat}) \pm 0.005(\text{syst})$, will remain the most precise determination of θ_{13} for the near future.

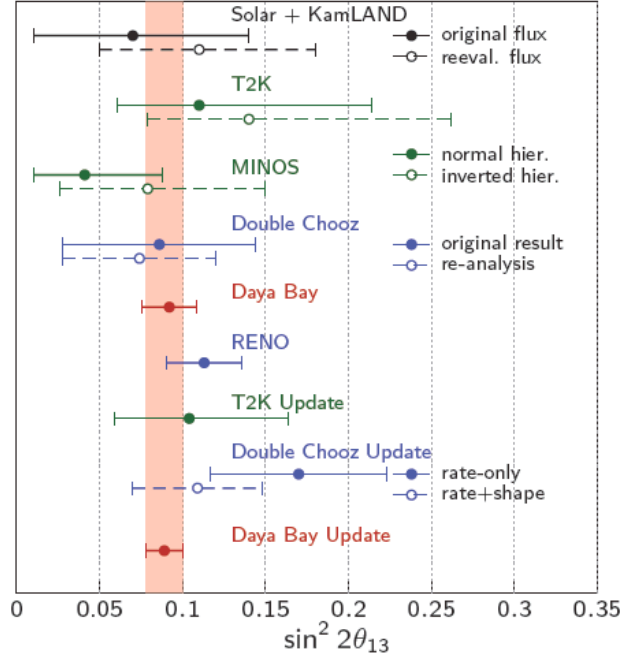


Figure 9. Summary of recent $\sin^2 2\theta_{13}$ measurements.

5. Summary

Within the last year our knowledge of $\sin^2 2\theta_{13}$ has gone from an upper bound to being the most precisely known of the neutrino mixing angles. The promise of the near/far experiment design has been fulfilled. Experimental errors are still dominated by statistics and we can confidently expect further error reduction in the coming years.

6. Acknowledgments

The Daya Bay experiment is supported in part by the United States Department of Energy, the Ministry of Science and Technology of China, the Chinese Academy of Sciences, the National Natural Science Foundation of China, the Guangdong provincial government, the Shenzhen municipal government, the China Guangdong Nuclear Power Group, Shanghai Laboratory for Particle Physics and Cosmology, the Research Grants Council of the Hong Kong Special Administrative Region of China, University Development Fund of the University of Hong Kong, the MOE program for Research of Excellence at National Taiwan University, National Chiao-Tung University, and NSC fund support from Taiwan, the U.S. National Science Foundation, the Alfred P. Sloan Foundation, the Ministry of Education, Youth and Sports of the Czech Republic, the Czech Science Foundation, and the Joint Institute of Nuclear Research in Dubna, Russia. We are grateful for the ongoing cooperation from the China Guangdong Nuclear Power Group and China Light & Power Company.

References

- [1] B. Pontecorvo, *Sov. Phys. JETP* 6 (1957) 429 and *Sov. Phys. JETP* 26 (1968) 984.
- [2] Z. Maki, M. Nakagawa, S. Sakata, *Prog.Theor.Phys.* 28 (1962) 870–880.
- [3] F. P. An et al. [Daya Bay Collaboration], *PhysRevLett.* 108(2012) 171803.
- [4] Y. Abe et al. [RENO Collaboration], *PhysRevLett.* 108(2012) 131801.
- [5] P. Adamson et al. [MINOS Collaboration], *Phys.Rev.Lett.* 107 (2011) 181802.
- [6] K. Abe et al. [T2K Collaboration], *Phys.Rev.Lett.* 107 (2011) 041801.
- [7] Y. Abe et al. [Double Chooz Collaboration], *PhysRevLett.* 108(2012) 131801.
- [8] Dan Dwyer, *Daya Bay Results, Neutrino 2012*, Kyoto, Japan.
- [9] Misaki Ishitsuka, *Double Chooz Results, Neutrino 2012*, Kyoto, Japan.
- [10] Y. Fukuda et al. [Super-Kamiokande Collaboration], *Phys. Rev. Lett.* 81 (1998) 1562–1567.
- [11] M.H. Ahn et al. [K2K Collab.], *Phys. Rev. D* 74, 072003 (2006).
- [12] D. Davis, Jr., D.S. Harmer, and K.C. Hoffman, *Phys. Rev. Lett.* 20, 1205 (1968).
- [13] Q. R. Ahmad et al. [SNO Collaboration], *Phys. Rev. Lett.* 89 (2002) 011301.
- [14] J.P. Cravens et al. [Super-Kamiokande Collab.], *Phys. Rev. D* 78, 032002 (2008).
- [15] Abe, S. et al. [KamLAND Collaboration], *Phys. Rev. Lett.* 100 (2008) 221803.
- [16] C. Bemporad, G. Gratta, Giorgio and P. Vogel, *Rev.Mod.Phys.* 74 297.
- [17] L. A. Mikaelyan and V.V. Sinev, *Phys. Atomic Nucl.* 63 (2000) 1002.
- [18] F.P. An et al. [Daya Bay Collaboration], *Nucl. Inst. and Meth.*A685, 78-97 (2012).
- [19] Soren Prell, *Observation of Electron-Antineutrino Disappearance at Daya Bay*, 1st Int. Conference on Frontiers in Physics, China, Greece 2012.